Letter to the Editor

The VLT observations of the HDF–S NICMOS field: photometric catalog and high redshift galaxy candidates

A. Fontana[1], **S. D'Odorico**[2], **R. Fosbury**[3], **E. Giallongo**[1], **R. Hook**[3], **F. Poli**[1], **A. Renzini**[2], **P. Rosati**[2], and **R. Viezzer**[2]

[1] Osservatorio Astronomico di Roma, via dell'Osservatorio, I-00040 Monteporzio, Italy
[2] European Southern Observatory, Karl-Schwarzschild-Strasse 2, D-85748 Garching, Germany
[3] Space Telescope – European Coordinating Facility, Karl-Schwarzschild-Strasse 2, D-85748 Garching bei München, Germany

Abstract. We present the deep $UBVRI$ observations of the HDF-S NICMOS field obtained as part of the Science Verification of the VLT Unit 1 telescope. The images have been used to construct object catalogs and to obtain photometric redshifts. The effective field of view is $\simeq 70 \times 70$ arcsec^2, and the formal 5σ limiting magnitudes (in a 2 FWHM aperture) are 26.3, 27.8, 27.5, 26.9, 25.2 in the U, B, V, R and I bands, respectively. Thanks to the sub-arcsecond image quality, relatively long exposure time, and large collecting area of the VLT, this is the deepest set of multicolor images ever obtained from a ground–based telescope.

Galaxy counts have been derived independently in each band, and show no significant departures from previous data from wider areas. A multicolor photometric catalog of all the galaxies selected in the R band has also been obtained and used to derive photometric redshifts for all galaxies with $R \leq 26.5$, using also the J,H and K magnitudes from the NICMOS deep observations. A significant fraction ($\simeq 28\%$) of the galaxies is placed at $z \geq 2$. Among them, six robust candidates are found at $z \geq 2.5$.

Key words: galaxies: general – cosmology: observations

1. Introduction

Deep imaging of extragalactic fields has long been recognized to be a powerful tool to understand galaxy evolution (see Ellis 1997 for an extensive review). Although faint galaxy counts have been of paramount importance to show that galaxies do evolve with redshift, the overall scenario and the physical processes that led to galaxy evolution are still debated. A new approach developed in recent years uses deep *multicolor* surveys to study the fainter magnitude galaxies: deep multi-band images are taken with a complete set of broad–band filters, in order to cover the overall spectrum of the galaxy and to discriminate the populations at

different redshifts. The Hubble Deep Field North (Williams et al. 1996) is the best–known examples of this kind of observations, but ground–based images have also been used, mainly to define sharp color criteria that select high–redshift galaxy candidates (Steidel et al 1995, Giallongo et al. 1998, Arnouts et al 1998).

This paper analyses deep observations of the Hubble Deep Field-South (HDF-S, Williams et al 1999) obtained in five colors (U, B, V, R and I) in August 1998 as part of the Science Verification phase of the first VLT 8.2m telescope (UT1). A description of the Science Verification programme at the VLT is to be found at http://www.eso.org/paranal/sv/.

The data have been taken for a field centered on $\alpha = 22h32m51.7$, $\delta = -60d38'48.2''$ (J2000), thus providing the optical complement to the near-IR J, H and K band images obtained with the HST NICMOS instrument (Fruchter et al 1999, see also http://www.stsci.edu/ftp/science/hdfsouth/hdfs.html), since the area covered by the optical observations is somewhat more extended than the NICMOS field of view.

This paper is organized as follows: In Sect. 2 we describe the data reduction procedures, while in Sect. 3 we discuss how the photometric catalogs were constructed. In Sect. 4 we derive the photometric redshifts for all the objects brighter than $R \simeq 26.5$ and discuss briefly their distribution at high redshift.

2. The data sample

2.1. Observations and data reduction

The data used here were retrieved from the ESO public archive, and refer to the observations that were obtained in the period August 17-September 1, 1998, using the VLT Test Camera (VLTTC) at the Cassegrain focus of the UT1. The VLTTC is a simple imaging camera which reimages the focal plane onto a 2048^2, 24 μm pixels, thinned SITe CCD. In the 2×2 binned mode which has been used for these observations the scale is 0.092 arcsec/pixel, giving a total field of 92×92 arcsec^2. For this program a set of several exposures through the standard $UBVRI$ Johnson-Cousin filters was obtained with single exposure integration times ranging from 600 to 1200 seconds.

LETTER

Table 1. Summary of the observational data

Filter	Number of frames	total exp. time (s)	Final PSF (FWHM) (arcsec)	Field of View (arcsec)×(arcsec) [1]	Zero-point [1]	Limiting Mag. (5 σ) [2]
U	16	17800	0.73	68.8×72.8	31.58	26.3
B	15	10200	0.78	71.7×71.7	33.13	27.8
V	16	14400	0.82	78×69.5	33.85	27.5
R	8	7200	0.64	72.6×66.9	34.06	26.9
I	12	10160	0.71	75.6×67.0	33.44	25.2

[1] Referred to the images released by ESO

[2] Magnitude limits are computed from the standard deviation of the sky counts inside apertures with diameters of $2 \times$ FWHM without aperture correction.

Airmass of individual exposures was always ≤ 1.4, with a median value of 1.25. Observations were obtained following the standard criteria for deep imaging, i.e. applying a slight offset between individual pointings to allow the removal of the detector imprints. Full details on the Test Camera, the CCD detector, the filter curves and on the individual exposures are available on the WEB site http://www.hq.eso.org/paranal/sv.

The data reduction has been carried out with different softwares at ESO and at the Rome Observatory. Although the two pipelines used completely independent environments and tools, they are quite similar in concept. Most of the steps are identical to those described elsewhere (e.g. Giallongo et al. 1998; Arnouts et al. 1998), and will not be repeated here. It is worth noting that flat-fielding is particularly critical in the VLTTC, since its CCD suffers from a very large blemish near the center and other lesser defects in the whole area. The central blemish is wavelength dependent, while variations from night to night caused by moving dust grains are also noticeable in the flats. Nevertheless, a satisfactory solution was finally found by constructing a separate "super-flat" as the median image of the unregistered images for each observing night. The final accuracy in flat–fielding is estimated to be better than 1%.

Only frames with seeing better than 1 arcsec were used in the final coaddition, without applying any drizzling algorithm (Fruchter and Hook 1998) since the VLTTC sampling is always much smaller than the seeing. As is customary in dithered multiple exposures, the edges of the final images are of poorer quality, since only a limited number of frames contribute to the observed flux. In the present observations the problem is noticeable because a large dithering pattern had to be applied to remove the blemishes and because of the small size of the field of view. Moreover, the central pointing of the coadded frames was not exactly the same in the different bands, which has further reduced the area common to all frames. We therefore used two different sets of images. In the first – that was part of the ESO public release – we trimmed the outer regions independently, keeping only the inner regions that were covered with 100% of the observations. These images were used to extract independent catalogs in each band.

We also produced a set of coadded images that are trimmed and aligned to the central field of the R frame, and these images were used to prepare the multicolor catalog. In practice, about 20% of this field is not covered by all the U and B frames, and therefore the coadded images are slightly shallower in these bands. The recently available images obtained by NICMOS with the F110W, F160W and F222M filters (Fruchter et al 1999) were also rebinned and aligned to the VLTTC R frame.

Table 1 summarizes the observational data that have been used, the FWHM of the PSF of the coadded single color images, their area, the photometric zero point, together with the formal 5σ limiting magnitudes. These were conservatively computed by taking the σ–clipped standard deviation of the sky counts in an aperture $2 \times$FWHM wide, taken at random positions on the images.

2.2. Photometric calibration

The photometric calibrations were obtained by reducing a series of standard stars from the Landolt (1992) sample. Self-consistent photometric solutions to the standard Johnson-Cousin system were derived for several individual nights, along with average solutions that use all the data from photometric nights. The zero points, color terms and extinction coefficients derived are listed at http://www.hq.eso.org/paranal/sv/html/data/photom.txt. We emphasize however that the coadded images presented here cannot be calibrated directly using the average coefficients, since they are the average of different exposures taken under various conditions.

A few isolated relatively bright stars have been selected in the field. Then, images obtained during each nights for which a photometric solution exists have been taken, and accurate magnitudes of the selected stars have been measured in each of these images. The resulting instrumental magnitudes have been converted into Johnson magnitudes using the photometric solution for the given night. Finally, each star has been assigned its average magnitude, after a σ–clipping removal of the discordant values.

The same photometry has been applied to the summed images, and the final zero point has been chosen in order to reproduce the magnitudes of the selected stars. We estimate that the final accuracy of this procedure is ~ 0.05 mags in each band. Finally, the zero points were corrected for galactic absorption with
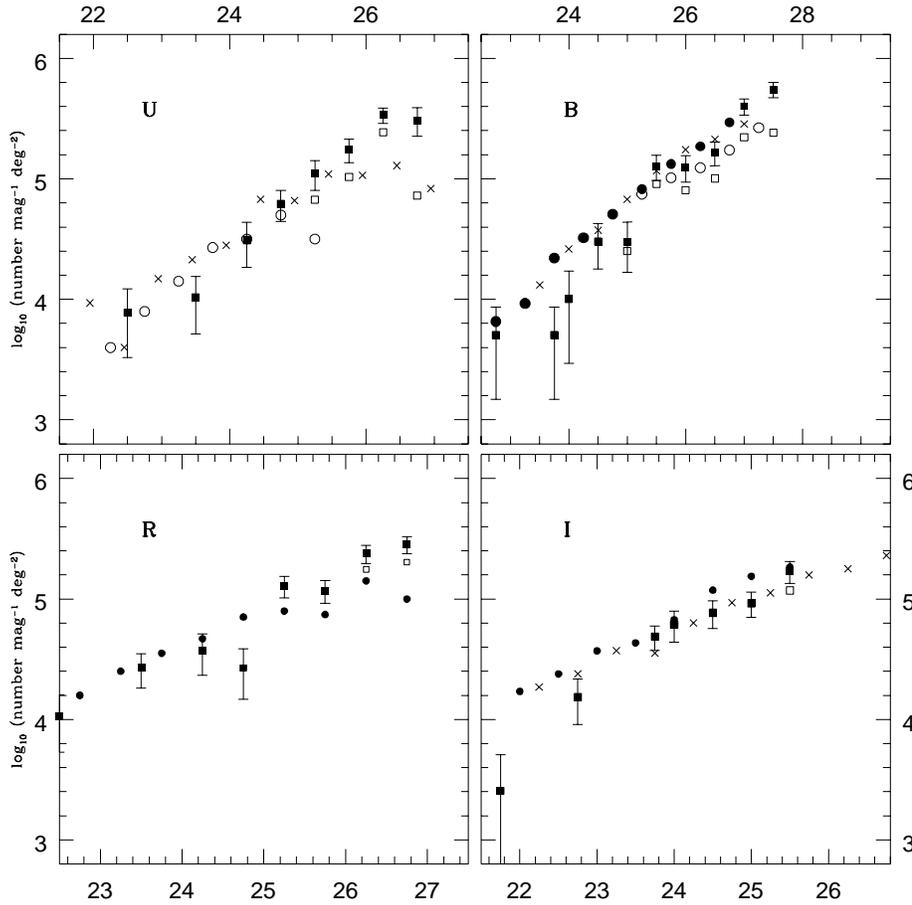
Fig. 1. Differential galaxy number counts for the U, B, R and I bands. VLT data are shown with open (raw) and filled (corrected) squares. Error bars take into account Poisson error only. Other data taken from the literature are shown. *U Band*: empty circles from Hogg et al 1995; crosses from HDF–N (Williams et al 1996). A correction $U_J = U_{AB} - 0.8$ has been applied to the latter data. *B Band*: (open) filled circles are (un–)corrected data from Metcalfe et al 1995a. Crosses from Arnouts et al 1998. *R Band*: Filled circles are raw Keck data from Smail et al 1995. *I Band*: Filled circles are from the NTT Deep Field (Arnouts et al 1998), crosses from HDF–N (Williams et al 1996).

$E(B - V) = 0.02$ (Burstein & Heiles 1982) with $\delta U = 0.095$, $\delta B = 0.084$, $\delta V = 0.063$, $\delta R = 0.05$, $\delta I = 0.038$.

3. The photometric catalog

The analysis of the two sets of images (the individual coadded images and those trimmed to the R band image) was performed using the SExtractor image analysis package (Bertin & Arnouts, 1996).

3.1. Galaxy counts

Within SExtractor, images were smoothed with a gaussian filter matching the seeing, and the detection threshold was chosen at 3σ of the background intensity in a contiguous area of 1 FWHM. Following Djorgovski et al. (1995), for each object both isophotal and aperture magnitudes (in a 2 FWHM aperture) were computed. The isophotal magnitude was used for the larger/brighter objects, i.e. for those objects where the isophotal area is larger than the aperture one. For fainter objects, an aperture correction to $5''$ has been estimated on bright stars and applied to correct the 2 FWHM aperture magnitude. This procedure is strictly valid for star-like objects only, but has been shown to be a good approximation on deep images (Smail et al. 1995).

Bright stars have been excluded from the catalogs using the CLASS_STAR parameter provided by SExtractor. A threshold CLASS_STAR< 0.9 has been set, on the basis of the comparison between ground–based and HST data (Arnouts et al 1998). At fainter magnitudes (e.g. $R \geq 24$) the neural network classifier does not work properly anymore, but stars are not expected to dominate the counts and therefore have been ignored. All the single-color catalogs are available on the web site http://www.mporzio.astro.it/HIGHZ.

A correction for incompleteness has been estimated in each band as in Arnouts et al. (1998), accounting for both false detection and the non–detection of real objects. We warn the reader that the correction for incompleteness has to be taken with some caution, because of the very limited size of the sample used as a reference. The raw and corrected counts in each band are shown in Fig 1, and compared to the most recent data from the literature. It is noteworthy here that the counts derived from these data are the deepest ever obtained from a single ground-based telescope, thanks to the sub-arcsecond image quality, relatively long exposure time and the large collecting area of the VLT.

3.2. The multicolor catalog

The multicolor catalog has been obtained from the set of aligned images, taking the R frame as reference. Object detection and
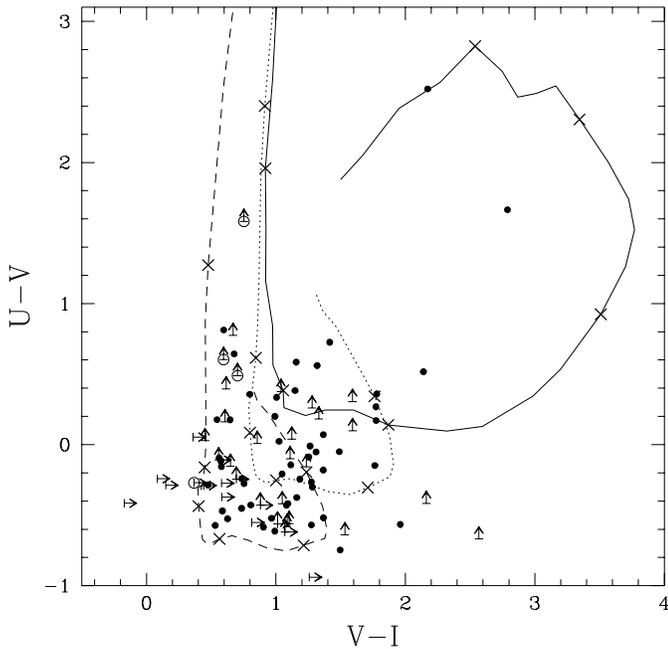
Fig. 2. The color distribution of galaxies in the VLT field. Points refer to galaxies in the $R \leq 26.5$ sample. Lower limits are shown at the 3σ level. Circles marks the objects at $z \geq 2.5$ selected from the photometric redshift. Overplotted are the evolutionary tracks of three galaxy templates, computed with a Miller–Scalo IMF and the following parameters: $\tau = 0.3$ Gyr, $z_{form} = 7$ and E(B-V)=0.1 (solid line); $\tau = 5$ Gyr, $z_{form} = 5$ and $E(B-V) = 0.2$(dotted line); $\tau = \infty$, $z_{form} = 5$, no dust (dashed line). Points at $z = 0.5, 1, 1.5, 2, 2.5, 3$ are marked by a cross.

the measurement of the R magnitude have been performed on the R frame exactly as described in the previous section. Then colors have been measured in a fixed circular aperture of 14 pixels (corresponding to 2 FWHM of the R frame), keeping the object position found on the R frame. To allow for the seeing difference among the coadded images, colors have been measured on images degraded to the $0.82''$ seeing of the V band image. The $R \leq 26.5$ subsample used for the following analysis consists of 91 galaxies and is available on the WEB http://www.mporzio.astro.it/VLT. The $R = 26.5$ threshold has been set in order to ensure good photometric accuracy and meaningful colors on the whole sample. Obvious stars have been excluded using the CLASS_STAR parameter (see above) in the R and – when available – in the NICMOS images.

Fig 2 shows the color distribution of the $R \leq 26.5$ sample in the $V-I$ vs $U-V$ plane. Overplotted on the observed colors are the evolutionary tracks of few galaxy templates as a function of redshift. They have been chosen to broadly encompass the most common spectral types, and are based on the synthetic models of Bruzual and Charlot (GISSEL library, 1996). It is clearly seen that a significant fraction of the faint galaxies has colors typical of star-forming galaxies at $z \simeq 2$, as expected in these very deep images (Metcalfe et al. 1995b). Though most of these objects are probably too faint for a spectroscopic confirmation with FORS or ISAAC at the VLT, their nature and redshifts
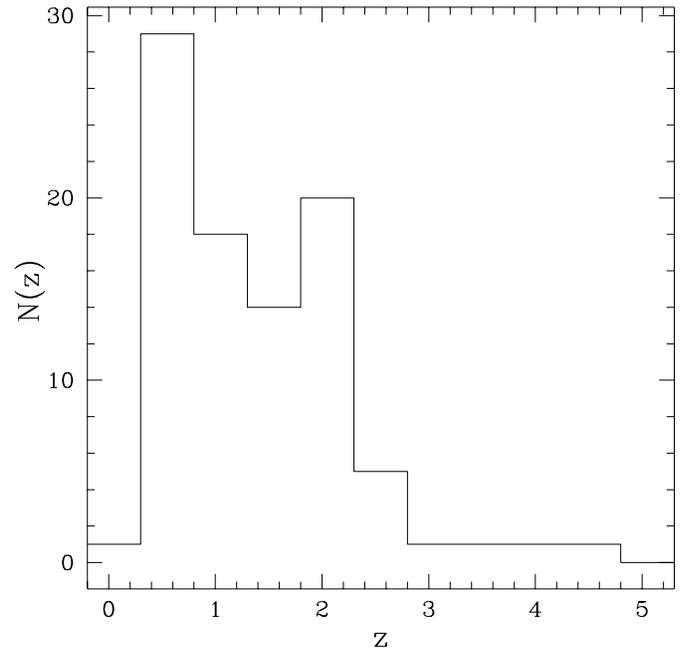

Fig. 3. The photometric redshift distribution of galaxies at $R \leq 26.5$ in the VLT field.

can be investigated further by means of a photometric redshift analysis.

4. The photometric redshifts of the $R \leq 26.5$ galaxies

The multicolor catalog has been used to derive photometric redshifts for all the 91 galaxies brighter than $R = 26.5$, using a technique extensively described elsewhere (Giallongo et al. 1998). In brief, we have computed the expected galaxy colors as a function of redshift for synthetic models in the GISSEL library, for an extensive variety of combinations of age, metallicity, IMF, and e-folding star formation time-scale. The reddening produced by internal dust in star-forming galaxies has then been added using the SMC extinction law (Pei 1992), along with the absorption produced by hydrogen in the intergalactic medium (Madau 1995). Finally, at any redshift galaxies are allowed to have any age smaller than the Hubble time at that redshift ($\Omega = 1$ and $H_0 = 50$ km s^{-1}Mpc^{-1} have been adopted throughout the paper).

The resulting large dataset includes $\simeq 5 \times 10^5$ "simulated galaxies", and a classical χ^2–minimization procedure has been applied to find the best-fitting spectral template to the observed colors.

This procedure has been tested on 108 galaxies with spectroscopically confirmed redshifts in the HDF-N (Cowie 1997; Cohen et al. 1997; Dickinson et al. 1997; Lowenthal et al. 1997 Fernadez–Soto et al 1998), obtaining an accuracy $\sigma_z \sim 0.1$ in the redshift interval $z = 0 - 3.5$ (Giallongo et al. 1998; Fontana et al. 1999).

The resulting redshift distribution is shown in Fig 3. A peak is clearly seen at $z = 0.5 - 1$, with a well populated tail extending to higher redshifts: about 28% of galaxies result indeed at $z \geq 2$.
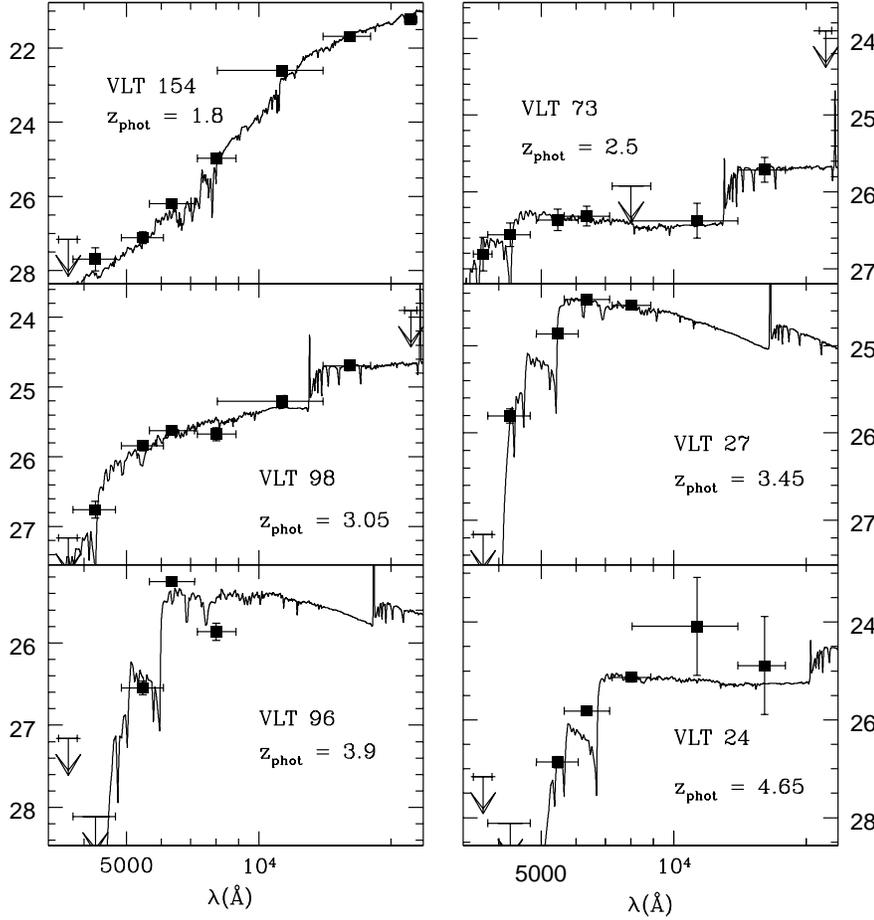
Fig. 4. The broad band energy distributions of high redshift galaxy candidates. Object VLT 154 was found by Treu et al 1998. Other objects are galaxies at $z \geq 3$ in the VLT field. Magnitudes have been converted into the AB system by $U_{AB} = U + .71$, $B_{AB} = B - 0.09$, $V_{AB} = V - 0.003$, $R_{AB} = R + .18$, $I_{AB} = I + .42$. The best–fitting spectrum is also shown.

A very red object was already identified as a $z \simeq 2$ candidate from the preliminary NICMOS observations, from being detected in the H band (F160W) and undetected in CTIO 4m telescope R and I band images with $(R - H)_{AB} > 3.9$ and $(I - H)_{AB} > 3.5$ (Treu et al 1998). This object (named VLT 154 in our catalog) is detected in all the VLT images except the U band, and our photometric redshift analysis indicates a redshift $z \simeq 1.8$ (see Fig 4). The redshift accuracy is limited by the lack of major spectral features, and acceptable solutions in the range $1.5 < z < 2.1$ can be found using different combinations of the parameters involved, consistent with the result of Stiavelli et al. (1998). The $z = 1.8$ best-fit is obtained with solar metallicity, $E(B - V) = 0.15$ (with a SMC extinction law), star–formation timescale $\tau = 0.3$ Gyr and an age of 2 Gyrs. Adopting the Calzetti (1997) extinction law we obtain $z = 1.65$ with $E(B - V) = 0.2$. Assuming no reddening from dust, we obtain an even higher best–fit redshift of $z = 2.05$. At $z = 1.8$, this object would have $M_K = -25.67$ and $M_B = -21.84$ (k–corrections are computed exactly from the best–fitting spectrum). Spectroscopic follow–up with ISAAC will hopefully reveal whether this object is indeed a high redshift elliptical galaxy undergoing passive evolution, as suggested by the fit parameters, a result that has a wide cosmological relevance.

The list of the objects at $z \geq 2.5$ is given in Table 2, while Fig. 4 shows the best fitting spectra of five of them. Two of these

Table 2. Galaxy candidates at $z \geq 2.5$

OBJ#	X [1]	Y [1]	R	z_{phot}
VLT 73	629.4	463.9	26.13	2.5
VLT 116	478.1	237.6	25.32	2.5
VLT 98	244.4	332.0	25.44	3.05
VLT 27	747.6	619.7	24.29	3.45
VLT 96	722.2	339.4	25.07	3.9*
VLT 24	64.7	630.5	25.64	4.65*

[1] Referred to the R image released by ESO
(*) Unresolved in the VLT images.

objects are unresolved in the VLT images, although they are too faint for the CLASS_STAR parameter to be reliable. Since they also fall outside the HST- STIS image overlapping the HDF-S NICMOS field, we are not able to exclude the possibility that they are actually galactic stars, that are the major source of interlopers in the Steidel et al. (1996) sample.

Before comparing these results to the HDF-N it is worth noting that HDF F300W filter is significantly wider and bluer than the Johnson U used here, with only a small overlapping region. As a result, the redshift range sampled by the HDF is wider and centered at a lower redshift ($2 < z < 3.2$) than in the present work ($2.5 < z < 3.4$), and the surface density of "U-

dropout" galaxies in HDF-N with $V_{606} \leq 26.5$ is significantly higher than found here, or $\simeq 18$ arcmin $^{-2}$ (Pozzetti et al. 1998).

Only one galaxy candidate at $z \geq 4$ results from the redshift distribution in Fig. 3. This is consistent with the number density of 0.8 arcmin^{-2} "B-dropout" galaxies detected in the HDF-N (Pozzetti et al. 1998) and lower than a similar prediction in the NTT-Deep Field (2.7 arcmin^{-2} at $r \leq 26$, Arnouts et al 1998).

Given the small size of the field studied with the VLT-TC these results are obviously of limited statistical significance. They demonstrate however the potential of future, wide field VLT instruments like FORS-1 and FORS-2, now planned to become operational in 1999 and 2000. These instruments will allow to explore to an unprecedented depth the distribution and evolutionary status of galaxies in the early universe.

References

Arnouts, S., D'Odorico, S., Cristiani, S., Zaggia, S., Fontana, A., Giallongo, E. 1998, A&A

Bertin, E., Arnouts, S. 1996, A&AS, 117, 393

Burstein, D., Heiles, C., 1982, AJ, 87, 1165

Calzetti, D. 1997, in "The Ultraviolet Universe at Low and High Redshift", astro-ph/9706121

Cohen et al 1996, ApJ, 471, L5

Cowie, L. L. 1997, http://www.ifa.hawaii.edu/cowie/tts/tts.html

Dickinson 1997, in the Hubble Deep Field, proceedings of the Space telescope Science Institute 1997 May Sympozium, eds. M. Livio, S.M. Falls, and P. Madau

Djorgovski S.G., Soifer, B., Pahre, M. et al., 1995, ApJ, 438, L13

Ellis, R. S., 1997, ARAA, 389

Fernandez–Soto, A., lanzetta, K., Yahil, A., 1998, astro-ph 9809126

Fontana, A. et al 1999, in prep.

Fruchter, A.S. & Hook, R.N. 1998, in "Applications of Digital Image Processing XX" ed. A. Tescher, Proc. S.P.I.E vol 3164, p120

Fruchter, A.S. et al, 1999, AJ to be submitt.

Giallongo,E., D'Odorico, S., Fontana, A. et al., 1998, AJ, 115, 2169

Hogg, D., Pahre, M., Mc Karthy, J., et al., 1997, MNRAS, 288, 404

Landolt, A.U., 1992, AJ, 104, 340

Lowenthal, J. D., Koo, D. C., Guzman, R., Gallego, J., Phillips, A. C., Faber, S. M., Vogt, N. P., Illingworth, G. D., Gronwall, C. 1997, ApJ 481, 673

Madau, P. 1995, ApJ, 441, 18

Metcalfe, N., Shanks, T., Fong, R., Roche, N., 1995a, MNRAS, 273, 257

Metcalfe, N., Shanks, Campos, A., R. Fong, J.P.Gardner 1995b Nature 383, 236 XXX

Pei, Y.C., 1992, ApJ, 395,130

Pozzetti, L., Madau, P., Zamorani, G., Ferguson, H.C., Bruzual, G., 1998, MNRAS 1133

Smail, I., Hogg, D. W., Yan, L., Cohen, J. G. 1995, ApJ, 449, L105

Steidel, C. C., Pettini, M., Hamilton, D., 1995, AJ, 110, 2519

Steidel, C. C., Giavalisco, M., Pettini, M., Dickinson, M., Adelberger, K. L. 1996, ApJ, 462, L17

Stiavelli, et al, A&A submitted

Treu et al, 1998, A&A Letter, 340, 10

Williams, R. E. et al. 1996, AJ, 112, 1335

Williams, R. E. et al. 1999, AJ to be submitted